



Research Article


Forging of an age-hardenable Mg–Al–Ca–Mn–Zn alloy on industrial scale



Nikolaus Papenberg¹  · Thomas Hatzenbichler² · Florian Grabner¹ · Peter J. Uggowitzer³ · Stefan Pogatscher³

Received: 10 August 2022 / Accepted: 28 November 2022

Published online: 12 December 2022

© The Author(s) 2022 

Abstract

Weight reduction plays an important role in transportation industries, directly impacting on fuel consumption and vehicle range. The use of multi-material mixes is common practice, allowing for an optimum application of specific material properties. Light metals, primarily aluminum alloys, are used in both, cast and wrought state, to good effect. On the other hand, magnesium alloys, which are still lighter by one third, are used in castings exclusively. While scientific research and development on Mg wrought alloys is progressing steadily, industrial implementation is still scarce. As a result, safety relevant and structural applications made from Mg wrought products are nearly nonexistent. To increase acceptance and facilitate industrial application for this interesting class of materials we investigated the forging process of an original-sized automotive control arm. To ease industrial access, the used age hardenable Mg–Al–Ca–Zn–Mn lean alloy, can be processed similarly to Al alloys, e.g. 6xxx series. This work describes the development sequence, starting with the analysis of the forming window, followed by laboratory forging trials and industrial sized part production, providing information on forming characteristics as well as possible difficulties.

Article Highlights

- The development sequence of a new Mg forging alloy, from material investigation to industrial forgings, is shown.
- Material behavior over a wide temperature range (250–500 °C) is evaluated.
- Life-sized automotive Mg parts are produced by closed die forging.

Keywords Magnesium wrought alloy · Mg–Al–Ca–Mn–Zn alloy · Closed die forging · Material characterization · Processing map

1 Introduction

Given the ever-increasing pressure on the transportation industries to improve vehicle fuel efficiency and range,

lightweighting is a topic of high interest. As light metals, especially Al alloys, are increasingly used in mid to high class cars [7], the industry has started to look for further optimization potential in terms of structural light

✉ Nikolaus Papenberg, nikolaus.papenberg@ait.ac.at; Thomas Hatzenbichler, thomas.hatzenbichler@krenhof.at; Florian Grabner, florian.grabner@ait.ac.at; Peter J. Uggowitzer, peter.uggowitzer@mat.ethz.ch; Stefan Pogatscher, stefan.pogatscher@unileoben.ac.at | ¹Light Metals Technologies Ranshofen GmbH, Austrian Institute of Technology, Lamprechtshausenerstr. 61, 5282 Ranshofen, Austria. ²Krenhof GmbH, Industriestr. West 2, 8605 Kapfenberg, Austria. ³Chair of Nonferrous Metallurgy, Montanuniversität Leoben, Franz-Josef Str. 18, 8700 Leoben, Austria.



metals. Mg alloys can provide a good combination of low weight and high specific properties for such structural applications. This has already been recognized for consumer electronics and various non-structural applications, where castings are in common use [11]. Nevertheless, the use of Mg wrought alloys, which can provide increased mechanical properties when compared to castings, is still lacking. This is mainly based on the large disparity in the production effort of castings versus wrought products made from Mg alloys. While the casting of complex geometries is appealing because of the good melt flow behavior of Mg [14], the deformation of Mg alloys is often considered problematic. This judgment is mainly based on the fact that forming has to be done at elevated temperatures, as well as on the lack of know-how resulting from the missing industrial utilization of Mg wrought products [9, 18].

To counteract this, scientific investigations concerning the production of sheets, extrusion and forgings made from Mg alloys are steadily increasing [29]. Nevertheless, the upscaling from laboratory trials to industrial production poses a multitude of challenges, which must be overcome.

To ease access of new materials for industrial applications, changes in standard production routines, such as processing and material handling, should be kept to a minimum. Therefore, a Mg alloy, which follows the same processing route as age-hardenable Al alloys (e.g. 6xxx series) has been chosen for industrial production trials by forging. Forgings allow for a broad variation of processing parameters by the interaction of material and die temperatures, forming speed and part complexity, thereby markedly increasing the process flexibility. Additionally, the processing of Mg alloys takes place at similar or slightly lower material temperatures when compared to Al forgings, further reducing complexity for industrial trials [4, 8, 10].

Age-hardenable Mg alloys, which have a similar processing sequence as Al alloys, consisting of casting, homogenization, forming operation, solution heat treatment and artificial ageing, have been well discussed in literature [19]. The resulting alloys are often characterized by a low amount of alloying elements to reduce solute drag and increase the available temperature window for solution heat treatment procedures. Also, there is a visible trend towards Ca containing alloys, allowing for a broad range of useable alloying elements. The used Mg–Al–Ca–Mn–Zn alloy (AXMZ1000) has a well-balanced elemental spectrum: Mn improves the corrosion behavior and is able to form dispersoids in combination with Al (e.g. Al_8Mn_5), stabilizing the grain structure at high temperatures [6]. The combination of Al and Ca provides the main hardening phase (Al_2Ca) [17] and Ca additionally

improves the oxidation resistance of the alloy [5]. Zn and Ca additions have been proven to reduce the texture intensity and therefore increase the ductility of Mg-alloys, which is an important effect for wrought alloys [2].

In this work, we illustrate the sequence of material analysis, laboratory trials and industrial scaled production of Mg forged parts, using an age-hardenable Mg–Al–Ca–Mn–Zn alloy with low overall alloying content.

2 Material and methods

Laboratory forging trials, heat treatments and analysis steps were done at Light Metals Technologies Ranshofen (LKR), industrial forging trials took place at Krenhof.

2.1 Material design

The used Mg-0.75Al-0.4Ca-0.3Mn-0.25Zn alloy (AXMZ1000), given in weight percent (wt.%), follows the trend of other age hardenable Mg alloys and has a low overall alloying content of 1.7 wt.%. This allows for a homogenization and solution heat treatment window in the range of approximately 480–530 °C, as Ca-containing phases can be dissolved adequately. This is of course not the case for the Mn containing phases, which are precipitated during homogenization at the latest and cannot be dissolved at the used processing temperatures. The artificial ageing is designed to make full use of the available Ca and Al in the Mg matrix, as hardening is enabled by precipitation of Al_2Ca precursor phases. The formation of the occurring phases is depicted in the thermodynamic equilibrium calculations, computed using Pandat™ software package, MatCalc database mc mg v1.006, given in Fig. 1.

2.2 Processing

Industrial produced ingots of AXMZ1000 alloy were remelted and cast into rectangular plates (570 × 45 × 300 mm) at LKR, using low pressure die casting. Forging stock with a size of 12 × 25 × 95 mm (rectangular) and $\varnothing 38 \times 541$ mm (round bar) was machined for the laboratory and the industrial trials, respectively. A three-step homogenization heat-treatment was done at material temperatures of 300 °C/3 h, 350 °C/2 h and 480 °C/4 h, and subsequently cooled at air. Laboratory sized piston rods were produced in a two-step isotherm forging process, which took place on a 160 t hydraulic forming press (DZP 160, Walter Neff Maschinenbau GmbH, Karlsruhe, Germany) with a ram speed of 10 mm s^{-1} . Forming was done at temperatures of 250, 300, 350, 400, 450 and 500 °C, the finished parts were cooled at air. An in-depth description of a comparable forging process, including a

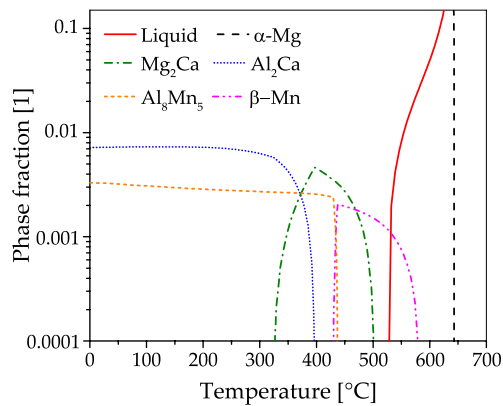


Fig. 1 Thermodynamic equilibrium calculations for the alloy AXMZ1000. Showing equilibrium phase fractions of α -Mg and the liquid as well as the intermetallic phases Al_2Ca , Mg_2Ca , Al_8Mn_5 and β -Mn as a function of temperature

time-temperature diagram (at 350 °C isothermal forming temperature) can be found in Ref. [20].

Forgings in the shape of an automotive control arm were produced in the industrial forging trials, using a three-step forming process, on a hydraulic press (LASCO Umformtechnik GmbH, Coburg, Germany) with a maximum press force of 1600 tonnes at Krenhof. A graphite-water lubricant, applied by spray gun, was used in all forging operations. Forged parts from both forming trials are depicted in Fig. 2. The produced parts were solution heat treated (490 °C/20 min./water quenched) and artificially aged to peak hardness, i.e. T6-temper (200 °C/1 h). All heat treatments were done at air using a laboratory sized forced convection chamber furnace (N120/85HA, Nabertherm GmbH, Lilienthal, Germany) at LKR.

2.3 Characterization

The processing behavior was characterized by microhardness measurements (LM 700 AT, LECO Corporation, St.

Joseph, MI, USA) and isothermal compression tests (Gleeble 3800-GTC, Dynamic Systems Inc., Poestenkill, NY, USA) in the range of 250 to 500 °C (step size of 50 °C) using cylindrical samples ($\varnothing 10 \times 12$ mm). The resulting flow curves were used to calculate a processing map as described in Sect. 2.4. The microstructure of the forged parts was analyzed by optical light microscopy (BX60, Olympus, Tokyo, Japan) and the grain size measured using line-intersecting method (ISO ASTM E112-13). Tensile testing was performed at room temperature (Z100, ZwickRoell GmbH & Co. KG, Ulm, Germany) acc. to EN ISO 6892-1, using flat specimens ($E 3 \times 8 \times 25$ mm) acc. to DIN 50125. The samples were taken from the center plane of the forgings, as indicated in Fig. 2b.

2.4 Processing map

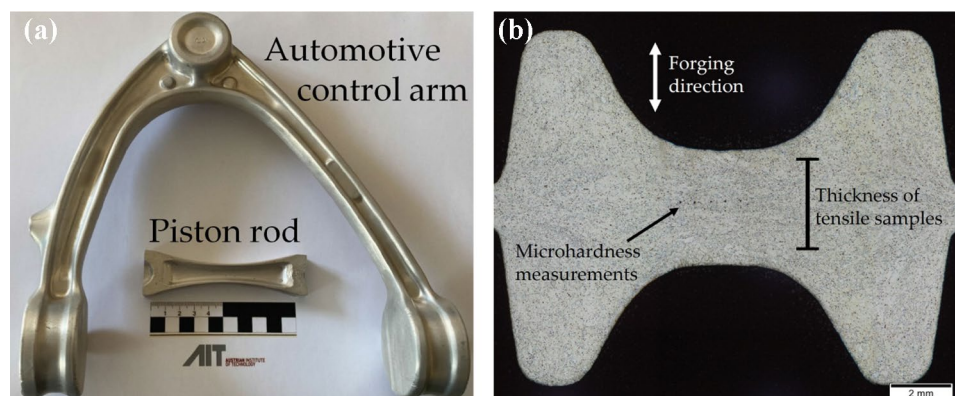
Processing maps are valuable tools to determine feasible process windows for forming operations. To create these maps, stress-strain curves at various strain rates and temperatures are used. The concept is based on the power dissipation rate (η) discussed in [22] and is derived from the strain rate sensitivity exponent (m), see Eqs. (1) and (2). At a fixed strain (φ), m is derived for various temperatures (T) and strain rates ($\dot{\varphi}$), reformulated as $\eta(T, \dot{\varphi})$ and depicted as a contour plot, see Fig. 3.

$$\eta = \frac{2m}{m+1}, \eta \leq 1 \quad (1)$$

$$m = \left. \frac{\partial \ln \sigma}{\partial \ln \dot{\varphi}} \right|_{\varphi} \quad (2)$$

As η describes the dissipation of kinetic energy during the forming process in heat and plastic deformation, a high power dissipation correlates to high deformation capabilities, which is desired for forming operations [30]. Thereby, a processing map allows for a good interpretation of favorable forming regions and expected process instabilities which must be avoided when designing forming

Fig. 2 Showing **a** Mg parts produced in laboratory (piston rod) and industrial sized forging (automotive control arm), **b** cross section of a piston rod (in T6-temper) and measurement positions



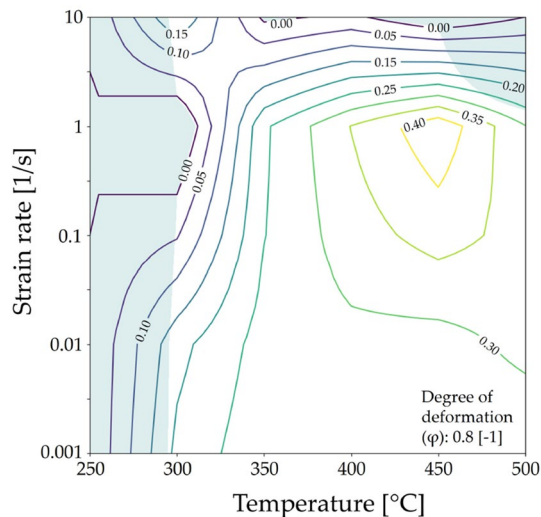


Fig. 3 Processing Map of AXMZ1000 alloy in the range of 250 to 500 °C and 0.001–10 s⁻¹, at a strain of 0.8 [- 1]. Contour lines show the power dissipation rate, shaded areas indicate instability domains

processes. These instabilities were interpreted using the failure criterion $2m < \eta$, introduced by Murty and Rao [16].

3 Results

3.1 Processing window

To obtain reliable indications of the possible forming parameters, isothermal compression tests were carried out over a broad range of temperatures and forming speeds, ranging from 250 to 500 °C and 0.001–10 s⁻¹. The samples tested at 250 °C showed shearing damage at low speeds while samples at 500 °C and a forming speed of 10 s⁻¹ broke by grain boundary failure. Otherwise, the alloy showed adequate results throughout, indicating good forming behavior in the temperature range of ~ 300–450 °C at the speeds used.

The resulting flow curves (not temperature compensated) were compiled into a processing map for easier interpretation and evaluation. This processing map, depicted in Fig. 3, shows two instability domains (shaded areas) and a wide range of possible forming parameters. The best forming behavior is calculated at 450 °C using a forming speed of 1 s⁻¹. The data is depicted at a strain of 0.8 [- 1] showing a relevant degree of deformation, as it corresponds to the local degree of deformation in the sample center of the parts produced in laboratory trials. As the compression tests and therefore the resulting processing map do not consider hydrostatic stresses, which are applied in closed die forging operations, the results can be considered as a worst-case scenario.

3.2 Laboratory forging trials

The findings of the processing map were evaluated in laboratory forging trials, producing piston rods in an isothermal forging process in two forming steps. To match industrial forming conditions the deformation speed of the laboratory trials was set to a ram speed of 10 mm s⁻¹, this also corresponds well to the maximum speed investigated in the compression tests. The forged parts verified the results of the processing map. While an optically sound piston rod was produced at 250 °C, the part formed at 500 °C fractured during the first forging step (see Fig. 4a). The reason for this was massive grain boundary failure in combination with insufficient lubrication of the forging die, caused by the evaporation of the used graphite-water lubricant on the hot die surface. Nevertheless, the parts formed at 250 °C have to be considered faulty, as shear fracture was detected in metallographic analysis (Fig. 4b). Therefore, the results of the preliminary compression tests and the calculated processing map were fully confirmed.

The trial sequence for the piston rods was completed with T6 heat treatment, and the parts were evaluated by microhardness test (HV0.1) and optical microscopy (OM). The microhardness measurements, shown in Fig. 5, provide an overview of the combined effect of forging and heat treatment parameters on the material properties. In the as-forged state the material hardness drops significantly with increased forging temperature. This behavior has a negligible effect on the material hardness in T6 state, which constantly remains on a high level. The largest effect of the age hardening treatment on the measured microhardness can be seen when comparing a solution heat treated (SHT) sample with the peak aged material, there an increase of ~ 25 HV0.1 is achieved.

In view of the experience gained in laboratory forging, the subsequent industrial forging trials were performed in a temperature regime of 300–450 °C, followed by T6 heat treatment of the formed parts.

3.3 Industrial forging trials

The industrial forged part (automotive control arm) was produced with a die used for Al forgings, at the same ram speed used in the regular production process. As Al forgings are usually not produced in isothermal forging, the permitted temperatures for this die were restricted to a maximum of ~ 200 °C. To counterbalance this low die temperature, the stock material was pre-heated to 450 °C before forming. The forging operation was done in three-steps, bending—pre-forging—final forging, without

Fig. 4 OM images of laboratory forged piston rods **a** grain boundary fracture at high forging temperature of 500 °C, **b** shear band damage during the forging at 250 °C

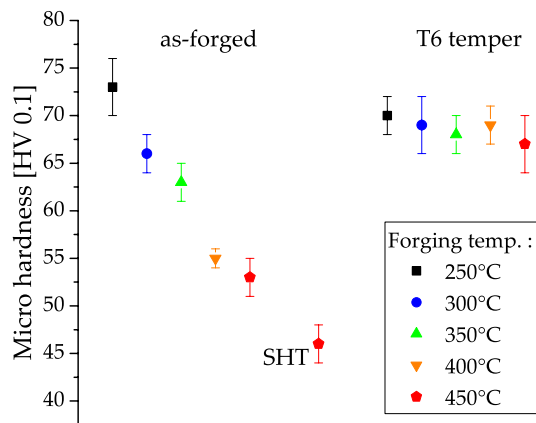
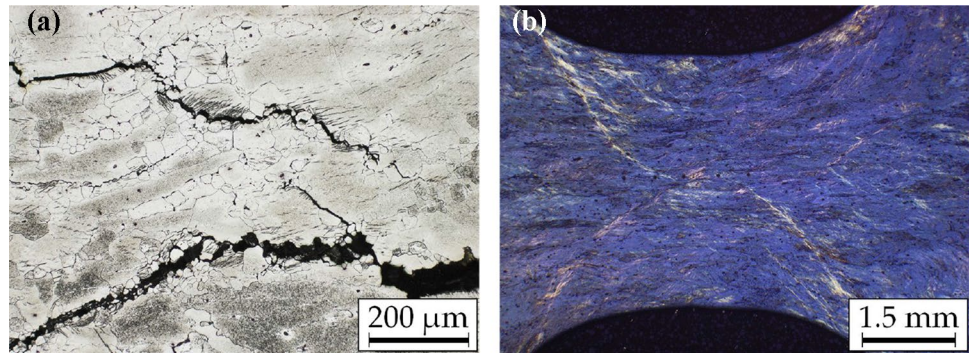


Fig. 5 Results from microhardness testing (HV0.1) of laboratory forged piston rods, showing as-forged, solution heat treated and peak aged material, including standard deviation

intermediate reheating. Finished parts were cooled at air and subsequently heat treated to peak hardness (T6).

3.4 Microstructure

The microstructural investigations of the laboratory forgings show a coherent picture throughout. In case of the as-forged material the amount of dynamically recrystallized (DRX) grains steadily increases with rising forging temperature. While the samples formed at 250 °C show shearing damage in the part center, twinning is visible throughout the microstructure of the 300 °C samples. In the parts formed at 350 and 400 °C dynamic recrystallization increases, progressing along twin and grain boundaries. This results in a mostly recrystallized microstructure at 450 °C forging temperature (Fig. 6). After T6 heat treatment of the laboratory forged piston rods, the microstructure of all samples is fully recrystallized (RX). Nevertheless, the differing forming temperatures can still be seen in the microstructure, as the grains coarsen with higher process temperatures. The grain size in the sample center thereby increases by over 60%, rising from 16 to 26 μm in diameter, see Fig. 6 and Table 1.

The microstructure of the industrially forged automotive control arm is shown in Fig. 7. The as-forged microstructure is permeated by twins and shows a low degree of DRX, mostly comparable to the piston rods forged at 300 °C. The T6 heat-treated material on the other hand shows a fully RX microstructure with a fine grain size, 11 μm in diameter.

3.5 Tensile properties

Tensile testing was done at room temperature for both, the isothermally forged piston rods and the industrially forged parts. The laboratory forgings show fluctuating mechanical properties with changing forming temperature. The highest tensile strengths were achieved at 400 °C. The industrially forged part in T6 temper shows the best overall properties, reaching an ultimate tensile strength (UTS) of ~ 260 MPa and a uniform elongation (ϵ_u) of > 7%, while the yield strength (YS) amounts to ~ 170 MPa. An overview of the mechanical properties and measured grain size of the peak aged parts is given in Table 1, representative stress-strain curves from tensile testing are depicted in Fig. 8.

4 Discussion

4.1 Processing window and laboratory forging trials

The preliminary investigations using compression testing and the calculation of the processing map indicate a good forming behavior in a broad processing window of 300–450 °C. This temperature range as well as the calculated power dissipation rate corresponds to literature available for Ca containing Mg alloys [23]. It is well known that the forming behavior and ductility in Mg alloys is strongly temperature dependent. This is caused by the large differences in critical resolved shear stress (CRSS) necessary for the activation of various slip systems. As these differences diminish with rising material temperature, the amount of available slip systems increases,

Fig. 6 OM images showing the microstructure of laboratory forged piston rods (part center) isothermally produced at 250 to 450 °C. The images show as-forged as well as peak aged material (T6-temper)

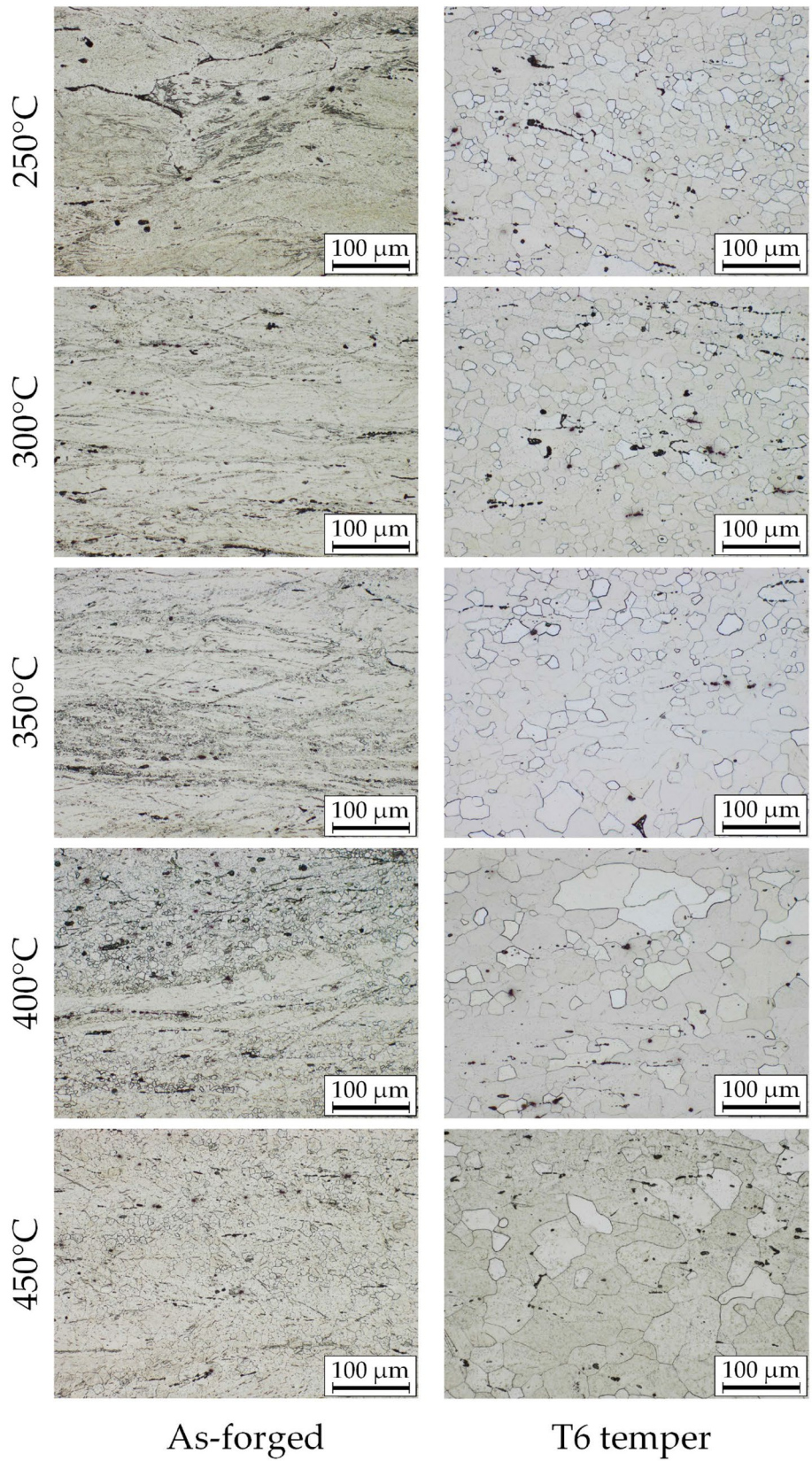


Fig. 7 Microstructure (OM images) of industrially forged automotive control arm in **a** as-forged state and **b** T6 temper

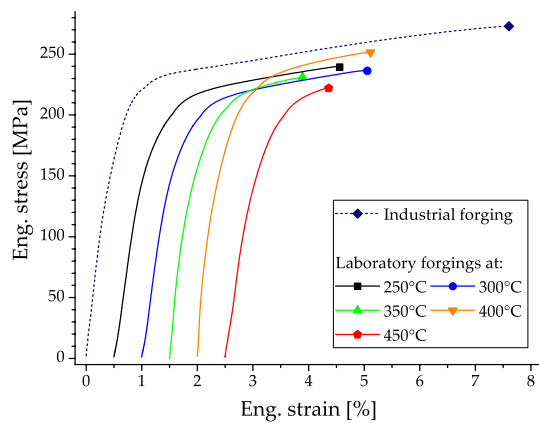
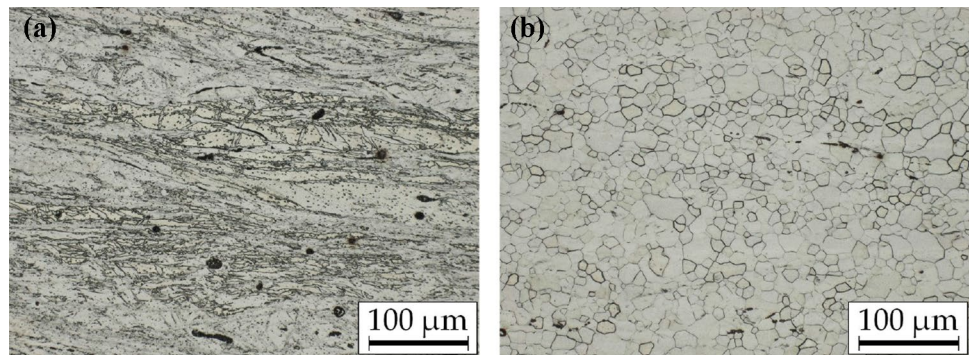


Fig. 8 Representative measurements from tensile testing of forged parts in T6 temper. For an improved overview the stress-strain curves are shifted by 0.5% eng. strain and fracture is marked by symbols

allowing for easier slip deformation and correspondingly enhanced ductility. At room temperature deformation processes are restricted to basal slip and twinning processes. Only at temperatures above 225 °C additional slip systems gradually become available [27]. This is the cause for the low deformation capabilities shown by the processing map at temperatures below 300 °C, regardless of the used forging speed, see Fig. 3. A slight improvement in forming behavior can be seen at a strain rate of 10 s⁻¹. At this

strain rate the sample temperature might be increased by the dissipated deformation energy [18], thereby enhancing the forming behavior. The same effect can be seen on the samples tested at 500 °C, while forming at low speeds is possible without problems, the material temperature increases at higher forming speeds, causing sample failure. As the solidus temperature of this alloy is at ~ 530 °C, see Fig. 1, and an increase in sample temperature of > 10 °C is likely, material failure is not surprising.

The best forming behavior, i.e. a η of 0.4, has been calculated at 450 °C and a strain rate of ~1 s⁻¹. As the processing map has been created with material data from cylindrical compression testing, the results can be considered as a lower limit. It is well known that material forming behavior can be improved by an increase in hydrostatic stresses during forming processes, such as closed die forging operations [18, 25]. Therefore, it can be assumed that the reduced formability caused by an increase in forging speed can be offset by the enhanced material ductility, provided by the hydrostatical stresses in closed die forging. Nevertheless, attention must be paid to processing at high forging temperatures, as an increase in material temperature must be expected which can cause material failure, as shown in the processing map at 500 °C and 10 s⁻¹.

The isothermal laboratory forging trials showed a good correlation to the results from compression testing and the processing map. The forging window in the range of 300–450 °C was confirmed using a ram speed of 10 mm s⁻¹,

Table 1 Microstructural and mechanical properties of AXMZ1000 forged parts in peak aged state (T6), including standard deviation

	Forging temp. [°C]	YS [MPa]	UTS [MPa]	Uniform elongation [%]	Micro hardness [HV0.1]	Grain diameter [μm]
Laboratory forgings	250	160 ± 7	226 ± 14	2.2 ± 1	70 ± 2	16 ± 2
	300	151 ± 2	235 ± 1	3.3 ± 0	69 ± 3	17 ± 3
	350	170 ± 3	229 ± 2	1.7 ± 0	68 ± 2	18 ± 2
	400	185 ± 2	247 ± 5	2.0 ± 1	69 ± 2	25 ± 6
	450	139 ± 1	230 ± 8	1.6 ± 0	67 ± 3	26 ± 5
Industrial forging		168 ± 2	258 ± 7	7.2 ± 1	69 ± 3	11 ± 1

producing well-formed piston rods without surface damage or internal forging defects.

To appraise the results of the processing map fully, also the limiting temperatures of 250 and 500 °C were investigated. While the piston rod forged at 250 °C was fully formed, shearing damage was found in the part center. This shows the positive effects of the applied hydrostatic stresses when compared to the compression samples, which fractured completely at lower strains. The isothermal forging at 500 °C failed after the first forging step, as the part ruptured in the center plane. This was most likely caused by the high processing temperature, which (i) facilitated grain boundary fracture and (ii) decreased lubrication effect on the surface of the forging die. Fracture along the grain boundaries, as shown in Fig. 4a, is not surprising as Mg–Ca alloys are known to have reduced grain boundary strength, caused by Ca segregation [21, 28]. Furthermore, the high forging temperatures, additionally increased by deformation heat, might cause incipient melting at locations with enrichment of alloying elements, e.g. grain boundaries.

4.2 Industrial forging trials

In case of Mg forming operations, the industry is often concerned with the conceived flammability of Mg alloys [9]. While Mg melts, chips and powders have to be handled with particular care, forming operations can be done with standard equipment. As Mg has a high heat transfer coefficient, industrial sized parts are usually able to dissipate heat from hot spots immediately; oxidation events are mainly found in areas where the heat transfer is reduced, e.g. edges and tips. Nevertheless, care has to be taken in case of high temperatures (e.g. homogenization) and machining [18].

To further alleviate industrial concerns, the used AXMZ1000 alloy has been shown to be stable at solution heat treatment conditions for 12 hours and allows temperature peaks up to the liquidus temperature for short periods in heat treatment trials performed at the LKR. Nevertheless, in case of Al processing industries, it should be mentioned, that a direct contact of Al and Mg parts during heat treatments must be avoided, as formation of $Mg_{17}Al_{12}$ phase in contact areas might occur. $Mg_{17}Al_{12}$ is a low melting eutectic phase (437 °C) [13], which can cause oxidation events in otherwise stable parts.

The industrial forging process setup was identical to the Al forgings of the automotive control arm: the same hydraulic press, forging die, lubrication and comparable forming speeds were used. The forging stock was formed without intermediate heat treatments, which are avoided in industrial settings whenever possible. Material flow behavior as well as die filling was adequate and no sticking

was observed in the three-step forging process, resulting in well-formed parts.

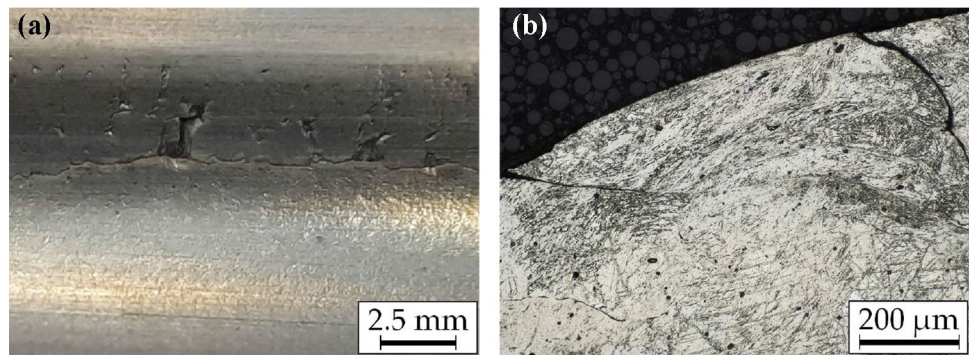
While the Mg forged parts were identical to Al forgings at a first glance, differences in the flash areas were visible. The forging flash of the control arm showed cracks, skewers, as well as sharp fractured edges. Small material flakes repeatedly broke away from the flash during forging operation. These fractures on the forging flash can be explained by two main factors: the high speeds at which the flash is formed, see [18, 24], and the reduction of temperature in this region, caused by small cross-sections and large surface areas. While this behavior poses a stark contrast to typical Al forgings, there was no detrimental effect on the forming process or part quality.

Further analysis of the forged Mg parts showed surface cracks, only visible after cleaning procedure (nitric acid 6 %) to remove the lubrication residue. These cracks were found on all forged parts, distributed over the whole surface, accumulating in areas of low part thickness and high exposure to the forging die, see Fig. 9. Additionally, shear band damage, comparable to Fig. 4b, was sporadically found in these areas as well. It may therefore be assumed, that the low die temperatures are responsible for these impairments. This is not wholly unexpected as the deformation behavior of Mg is markedly reduced below 250 °C, fully relying on basal slip and twinning [3].

While the heat transfer of Al and Mg is comparable, the heat capacity of Mg is lower than Al. Therefore, the heat transferred from the part into the forging die has a larger effect on the temperature of the Mg part. This would confirm the effect of the low die temperature: material temperature reduction occurs in areas of low part thickness and high exposure to the (colder) forging die, where cracks were mostly found. Additional confirmation can be found in the laboratory forgings, as such surface damage did not occur in the isothermally produced piston rods. The die temperature during laboratory forgings was 250 °C minimum, while the temperature in the industrial forging die was still lower at 150 °C.

Deburring of Al parts is usually done using a deburring die, which removes the flash material and trims the part to the desired size. This takes place at room temperature for ease of handling and to avoid sticking / smearing of the material during removal. This process cannot be identically replicated with Mg parts, as the flash areas tend to fracture brittle in case of room temperature removal, which might cause the fracture to extend into the part itself. Additionally, the part size may differ from the Al parts as the used forging temperatures and the heat expansion coefficient are different. The forged Mg parts were therefore deburred using a band saw, which is an adequate alternative in case of small lot sizes.

Fig. 9 Images of the automotive control arm showing **a** cracks on part surface **b** OM image of crack propagation in the part interior



Heat treatment (T6-temper) was done with the same parameters as applied to the laboratory forgings. There is a distinct difference in part thickness within the forged control arm, as well as in comparison to the piston rods. To investigate effects caused by this difference in cross-section, comparative temperature measurements were done during solution heat treatment, as it is the most critical heat treatment step in this regard (high temperature, short treatment times). Only a difference of ~ 1 min was measured between the thickest and thinnest part of the automotive control arm in reaching the solution heat treatment temperature. Obviously, the good heat conduction of Mg makes this problem mostly irrelevant for the used part sizes. A major difference between the T6 heat treatment of Mg and Al parts is the missing effect of natural ageing in case of the Mg forgings [15, 26], which simplifies the sequential arrangement of the heat treatments accordingly.

4.3 Microstructure and mechanical properties

The microstructure of all laboratory forged parts, in as-forged state, is directly dependent on the forming temperature: with rising temperature the amount of DRX-grains increases, while the number of deformed grains from casting is reduced, compare Fig. 6. This behavior is confirmed by microhardness measurements, given in Fig. 5. The hardness is reduced with increasing forming temperature, as the microstructure increasingly recrystallizes and defect hardening is diminished [10]. The as-forged microstructure of the industrially produced parts cannot directly be correlated to a forging temperature, as it is created by the combination of different material and die temperatures. Here, mostly deformed grains and twinning structures are visible. Such a structure is strongly dependent on the degree of deformation, which facilitates either fracture at twin boundaries or DRX, depending on the forming temperature [1].

Of higher interest is the microstructure of the parts in T6-state, where a fully recrystallized grain structure can be found, see Fig. 6. The DRX grains are enlarged during the heat treatment while the deformed remnants of the cast microstructure are replaced by new statically recrystallized grains. This recrystallization process is dependent on the applied heat treatment temperatures (here 490°C), as well as on the deformation present in the microstructure. The deformation provides both, starting points and stored energy for the static recrystallization [12]. Thereby explaining the dependence of the resulting grain size on the microstructure created during the forging process. Accordingly, the smallest grain size is achieved by the industrially forged part, which has a high amount of deformed grains but only a small proportion of DRX in the as-forged microstructure, see Fig. 7. This results from low forming temperature and high degree of deformation, up to a local degree of deformation of ~ 5 .

Tensile properties in peak aged state vary for all forged parts due to the differing forming temperatures, e.g. the YS ranges between 140 and 185 MPa. The lowest value was measured for the parts isothermally forged at 450°C . These forgings show the highest fraction of dynamically RX grains during the forging process as well as the largest grain size. Mg alloys benefit strongly from small grain sizes, as they have high Hall-Petch constants, i.e. k_y of $250\text{ MPa } \mu\text{m}^{-1/2}$ [6]. Nevertheless, large strength improvements by grain boundary hardening primarily take place at grain diameters below $\sim 5\text{ }\mu\text{m}$, therefore only differences of smaller 25 MPa YS can be expected in the produced parts.

While the main hardening effect in the discussed samples clearly stems from precipitation hardening, as visible in Fig. 5, also the forming texture can play an important part. The strong basal texture developed in Mg wrought alloys is often reported to have noticeable impact on the mechanical behavior [2], thereby playing an important role on both the achievable YS and ductility. The YS can be improved by high basal intensities if

the applicable Schmid factors are reduced. On the other hand, a low texture intensity can be associated with an improved ductility, by allowing for a more heterogeneous distribution of slip directions. Especially parts produced by directional processes, i.e. rolling and extrusion, are known for their sharp textures, which are less pronounced in forgings. Additionally, the overall texture of the discussed forged parts is markedly reduced by the heat treatment processes, as discussed in [20]. However, a noticeable impact on material properties must also be assumed here. This is affirmed by a comparison with the stable microhardness values in T6 temper, which are less affected by differences in the texture when compared to tensile measurements.

The industrial forgings show low grain sizes and a higher degree of deformation when compared to the laboratory forgings, this is reflected in their good YS, but especially in the high ϵ_u reached (>7 %). The superior UTS (~ 260 MPa) of these samples is most likely linked to the ductility, which is the highest value achieved in this investigation. The elongation of the forged parts is mainly controlled by element enrichment and phases at the grain boundaries, which may cause premature fracture. Nevertheless, when comparing the tensile properties of the industrially sized Mg part to the performance of the Al part produced in the standard process, adequate specific properties are reached. The Al forgings reach minimum YS and UTS values of 300 and 340 MPa, respectively. Accordingly, the specific strength values of the Al and Mg parts deviate by ~ 15%, showing possible improvements by weight parity design. Note, that an increase of the elongation, YS and UTS of the AXMZ1000 parts seems achievable by using extruded forging stock [20].

5 Conclusion

The necessary production steps of Mg forged parts were analyzed in this work. Thereby, we investigated the (i) material selection, (ii) determination of suitable process parameters (by means of compression test), (iii) laboratory and (iiii) industrial scaled forging trials including heat treatment procedures. The lessons learned can be summarized as follows:

- The use of isothermal compression testing and the subsequent calculation of a processing map for the used AXMZ1000 alloy reveal a forming window in the range of 300–450 °C, at strain rates of 0.001 to 10 s⁻¹.
- Laboratory forging trials verify the results from compression testing and enable the achievement of reproducible component qualities with stable hard-

ness values (HV0.1) after T6 heat treatment, regardless of the used forming temperature.

- Automotive control arms were successfully produced in industrial forging trials. Favorably, with the lean Mg alloy used, large variations in material and mould temperatures are possible.
- The die temperature has proven to be a limiting factor for the production of Mg forgings, which can lead to surface cracks if it is chosen too low.

It can be concluded that the step from Al industrial forgings to the production of Mg parts made from AXMZ1000 alloy is straightforward. Existing forging and heat treatment equipment can be used without problems, solely the die temperatures have to be raised accordingly. Nevertheless, special care must be taken to avoid material mix-ups, as Al processing conditions are unsuitable for Mg parts and can cause oxidation events. This must be kept in mind also for the following production steps, such as cleaning and machining.

Acknowledgements The authors would like to thankfully acknowledge the work done by the technical staff at the LKR Ranshofen. Furthermore, we would like to thank Krenhof for conducting the industrial forging trials and the institute of metal forming at MU Leoben for performing compression tests.

Author contributions Conceptualization: NP, PJU; Methodology: FG; Formal analysis and investigation: NP; Writing—original draft preparation: NP; Writing—review and editing: NP, TH, FG, PJU, SP; Funding acquisition: SP; Resources: TH; Supervision: PJU, SP.

Funding We gratefully acknowledge the financial support of this work within the scope of the AMALFI project. AMALFI is a COMET Project within the COMET–Competence Centers for Excellent Technologies Program and funded by BMK, BMDW, and the federal state of Upper Austria. The COMET Program is managed by the FFG (grant number 872641).

Data availability The raw/processed data required to reproduce these findings cannot be shared at this time as the data also form part of an ongoing study.

Declarations

Conflict of interest The authors have no competing interests to declare that are relevant to the content of this article.

Open Access This article is licensed under a Creative Commons Attribution 4.0 International License, which permits use, sharing, adaptation, distribution and reproduction in any medium or format, as long as you give appropriate credit to the original author(s) and the source, provide a link to the Creative Commons licence, and indicate if changes were made. The images or other third party material in this article are included in the article's Creative Commons licence, unless indicated otherwise in a credit line to the material. If material is not included in the article's Creative Commons licence and your intended use is not permitted by statutory regulation or exceeds the permitted use, you will need to obtain permission directly from the copyright

holder. To view a copy of this licence, visit <http://creativecommons.org/licenses/by/4.0/>.

References

1. Al-Samman T, Gottstein G (2008) Dynamic recrystallization during high temperature deformation of magnesium. *Mater Sci Eng A* 490(1–2):411–420. <https://doi.org/10.1016/j.msea.2008.02.004>
2. Basu I, Chen M, Wheeler J et al (2021) Stacking-fault mediated plasticity and strengthening in lean, rare-earth free magnesium alloys. *Acta Mater* 211:116877. <https://doi.org/10.1016/j.actamat.2021.116877>
3. Bettles C, Barnett M (2012) *Advances in wrought magnesium alloys: fundamentals of processing, properties and applications*. Elsevier
4. Birol Y, Ilgaz O, Akdi S et al (2014) Comparison of cast and extruded stock for the forging of AA6082 alloy suspension parts. In: *Advanced materials research*. Trans Tech Publ, pp 299–304
5. Choi BH, You BS, Park WW et al (2003) Effect of Ca addition on the oxidation resistance of AZ91 magnesium alloys at elevated temperatures. *Met Mater Int* 9(4):395–398. <https://doi.org/10.1007/BF03027194>
6. Cihova M, Schäublin R, Hauser LB et al (2018) Rational design of a lean magnesium-based alloy with high age-hardening response. *Acta Mater* 158:214–229. <https://doi.org/10.1016/j.actamat.2018.07.054>
7. Czerwinski F (2021) Current trends in automotive lightweighting strategies and materials. *Materials* 14(21):6631. <https://doi.org/10.3390/ma14216631>
8. Drossel G, Friedrich S, Kammer C et al (2018) *Aluminium Taschenbuch 2: Umformung, Gießen, Oberflächenbehandlung, Recycling*. Beuth Verlag
9. D’Errico F, Tauber M, Just M (2022) Magnesium alloys for sustainable weight-saving approach: a brief market overview, new trends, and perspectives. In: Sunkari S (ed) *Current trends in magnesium (Mg) research*. IntechOpen
10. Emley EF (1966) *Principles of magnesium technology*. Pergamon Press, Oxford
11. Kainer KU (2019) 40 years of magnesium research—Assessment of contribution to the progress in magnesium technology. In: 79th annual IMA world magnesium conference, Budapest. International Magnesium Association
12. Li Z, Sasaki T, Bian M et al (2020) Role of Zn on the room temperature formability and strength in Mg-Al-Ca-Mn sheet alloys. *J Alloys Compd* 847:156347. <https://doi.org/10.1016/j.jallcom.2020.156347>
13. Liang P, Su HL, Donnadiou P et al (1998) Experimental investigation and thermodynamic calculation of the central part of the Mg-Al phase diagram. *Int J Mater Res* 89(8):536–540
14. Luo AA (2013) Magnesium casting technology for structural applications. *J Magnes Alloys* 1(1):2–22. <https://doi.org/10.1016/j.jma.2013.02.002>
15. Mima G, Tanaka Y (1971) The aging characteristics of magnesium-4wt% zinc alloy. *Trans Jpn Inst Met* 12(2):71–75
16. Murty SN, Rao BN (1998) On the development of instability criteria during hotworking with reference to IN 718. *Mater Sci Eng A* 254(1–2):76–82. [https://doi.org/10.1016/S0921-5093\(98\)00764-3](https://doi.org/10.1016/S0921-5093(98)00764-3)
17. Nie JF (2012) Precipitation and hardening in magnesium alloys. *Metall Mater Trans A* 43(11):3891–3939. <https://doi.org/10.1007/s11661-012-1217-2>
18. Papenberg NP, Gneiger S, Weißensteiner I et al (2020) Mg-Alloys for forging applications-A review. *Materials* 13(4):985. <https://doi.org/10.3390/ma13040985>
19. Papenberg NP, Gneiger S, Uggowitz PJ et al (2021) Lean wrought magnesium alloys. *Materials* 14:4282. <https://doi.org/10.3390/ma14154282>
20. Papenberg NP, Arnoldt A, Trink B et al (2022) Closed die forging of a Mg-Al-Ca-Mn-Zn lean alloy. *Mater Sci Eng A* 857:144079. <https://doi.org/10.1016/j.msea.2022.144079>
21. Pei R, Zou Y, Wei D et al (2021) Grain boundary co-segregation in magnesium alloys with multiple substitutional elements. *Acta Mater* 208:116749. <https://doi.org/10.1016/j.actamat.2021.116749>
22. Rao K, Prasad Y, Sivaram K (1990) Deformation processing map for control of microstructure in Al-4Mg alloy. *Mater Lett* 10(1–2):66–70. [https://doi.org/10.1016/0167-577X\(90\)90016-F](https://doi.org/10.1016/0167-577X(90)90016-F)
23. Rao KP, Prasad YVRK, Dharmendra C et al (2018) Review on hot working behavior and strength of calcium-containing magnesium alloys. *Adv Eng Mater* 20:1701102. <https://doi.org/10.1002/adem.201701102>
24. Sabroff A, Boulger F, Henning H et al (1964) *A manual on fundamentals of forging practice*. Tech. rep
25. Skubisz P, Sińczak J (2007) Precision forging of thin-walled parts of AZ31 magnesium alloy. *Arch Metall Mater* 52(2):329–336
26. Sturkey L, Clark J (1959) Mechanism of age-hardening in magnesium-zinc alloys. *J Inst Met* 88(177–181)
27. Suresh K, Rao K, Prasad Y et al (2014) Study of hot forging behavior of as-cast Mg-3Al-1Zn-2Ca alloy towards optimization of its hot workability. *Mater Des* 57:697–704. <https://doi.org/10.1016/j.matdes.2014.01.032>
28. Trang T, Zhang J, Kim J et al (2018) Designing a magnesium alloy with high strength and high formability. *Nat Commun* 9(1):1–6. <https://doi.org/10.1038/s41467-018-04981-4>
29. Zeng Z, Stanford N, Davies CHJ et al (2019) Magnesium extrusion alloys: a review of developments and prospects. *Int Mater Rev* 64(1):27–62. <https://doi.org/10.1080/09506608.2017.1421439>
30. Zhou G, Ding H, Cao F et al (2014) A comparative study of various flow instability criteria in processing map of superalloy GH4742. *J Mater Sci Technol* 30(3):217–222. <https://doi.org/10.1016/j.jmst.2013.07.008>

Publisher’s Note Springer Nature remains neutral with regard to jurisdictional claims in published maps and institutional affiliations.